Research Square

Preprints are preliminary reports that have not undergone peer review.
They should not be considered conclusive, used to inform clinical practice,
or referenced by the media as validated information.

Defect induced site-selective self-trapped holes and their optical fingerprints in β-Ga2O3.

F. Bermúdez-Mendoza
Complutense University of Madrid
E. Nogales
Complutense University of Madrid
B. Méndez
Complutense University of Madrid
F. Domínguez-Adame
Complutense University of Madrid
E. Díaz
Complutense University of Madrid
R. Martínez-Casado
mariarum@ucm.es
Complutense University of Madrid

Article

Keywords:

Posted Date: April 27th, 2026

DOI: https://doi.org/10.21203/rs.3.rs-9008105/v1

License: This work is licensed under a Creative Commons Attribution 4.0 International License.
Read Full License

Additional Declarations: No competing interests reported.

Defect induced site-selective self-trapped holes and their optical fingerprints in β-Ga_2O_3

F. Bermúdez-Mendoza, E. Nogales, B. Méndez, F. Domínguez-Adame, E. Díaz,* and R. Martínez-Casado†
Department of Materials Physics, Complutense University of Madrid, E-28040 Madrid, Spain

The monoclinic β-Ga_2O_3 exhibits strongly linearly polarized ultraviolet luminescence, associated to native defects; however, the microscopic relationship between the tetrahedral (VGa_I) and octahedral (VGa_{II}) native gallium vacancies and the observed optical dichroism remains unresolved. By considering spin-polarized hybrid density-functional theory, we demonstrate that both gallium vacancies act as efficient traps for oxygen-centered self-trapped holes (STHs). Specifically, VGa_I and VGa_{II} favor different STH configurations localized on inequivalent neighboring oxygen sites, that lead to spin-polarized weakly dispersive defect states closed to the valence-band maximum. These energy levels allow for defect-specific optical transitions to the conduction-band. Thus, the anisotropic real-space STH wavefunctions, dictated by the local Ga-O connectivity, induces a pronounced vacancy-dependent linear dichroism in the near-edge optical response. In this work we establish a correlation between the polarization-resolved optical spectra and the particular spatial distribution of STH generated in presence of the two possible gallium-vacancies in β-Ga_2O_3 to provide a unified microscopic interpretation of its UV defect luminescence.

I. INTRODUCTION

Ultrawide bandgap semiconductors (UWBG) are central to the next generation of high-power and UV optoelectronic devices [1]. Among them, monoclinic β-Ga_2O_3 has emerged as a flagship material due to its large gap ($\sim$4.5-4.9 eV), chemical robustness, availability of bulk substrates and controllable n-type doping [2–7]. These properties have already enabled working prototypes of Schottky barrier diodes, field-effect transistors, scintillators, and solar-blind photodetectors [2, 8–14], and drive intensive research efforts to engineer its defect and doping properties for both power electronics and UV optoelectronics [15–18].

β-Ga_2O_3 crystallizes in a monoclinic lattice that hosts two inequivalent Ga sublattices: the tetrahedral, fourfold-coordinated Ga_I bonded to four oxygen atoms, and the octahedral, sixfold-coordinated Ga_{II} bonded to six oxygen atoms as shown in Fig. 1(a) [7]. This low symmetry leads to pronounced anisotropy in the electronic structure and optical response, including birefringence, direction-dependent absorption edges, and polarization-selective luminescence [4, 19–22]. Recent X-ray excited optical luminescence (XEOL) experiments on nanomembranes with a surface normal along (100) revealed UV emission that is strongly polarized along (001), together with blue and deep-UV bands attributed to Ga-vacancy–induced states [23].

At the microscopic level, many of the exotic optoelectronic properties of β-Ga_2O_3 are now understood to be governed by self-trapped holes (STHs). Holes in β-Ga_2O_3 tend to localize on individual oxygen ions, accompanied by a local lattice distortion [24], rather than forming extended Bloch states. Hybrid density functional theory (DFT) calculations and electron-paramagnetic-resonance (EPR) experiments have established STHs centered on three-fold coordinated O atoms in the pristine lattice, with trapping energies of several tenths of electron-volt and characteristic local structural relaxations [25–29]. Similar behavior has been identified across many UWBG oxides and is known to strongly limit hole mobility and to reshape radiative and nonradiative recombination pathways [30].

These STHs can be tracked through luminescence spectroscopy. In unintentionally doped β-Ga_2O_3 crystals and films, a broad UV band around 3.1-3.4 eV is commonly ascribed to the recombination of conduction-band (or shallow-donor) electrons with self-trapped holes [25, 26, 31]. Additional blue and green bands are generally interpreted in terms of donor–acceptor pair transitions involving native defects and unintentional impurities, although detailed assignments remain controversial [16, 18, 32–34]. Cathodoluminescence (CL), photoluminescence (PL) and XEOL studies on nanowires, nanostructures, and nanomembranes have revealed that these broad bands often coexist with discrete defect levels that allow for strong thermal quenching due to the underlying STHs and migration processes [23, 35–38].

Controlling these STHs states is crucial for both luminescence and electrical conductivity engineering. In β-Ga_2O_3, the deep valence band and the strong propensity for hole self-trapping render p-type conductivity notoriously difficult to achieve. This remains the case despite extensive investigations of acceptor dopants (e.g., Mg, Zn, N) and more recent co-doping or alloying approaches [30, 37, 39–41]. By contrast, n-type conductivity is readily obtained, typically through substitutional donor impurities such as Si, Ge, or Sn, with unintentional Si often dominating the background carrier concentration [16, 42].

Native point defects provide an additional powerful lever for tuning the optoelectronic properties. First-principles calculations and experimental studies now con-

* elenadg@fis.ucm.es; Corresponding author
† mariarum@ucm.es; Corresponding author

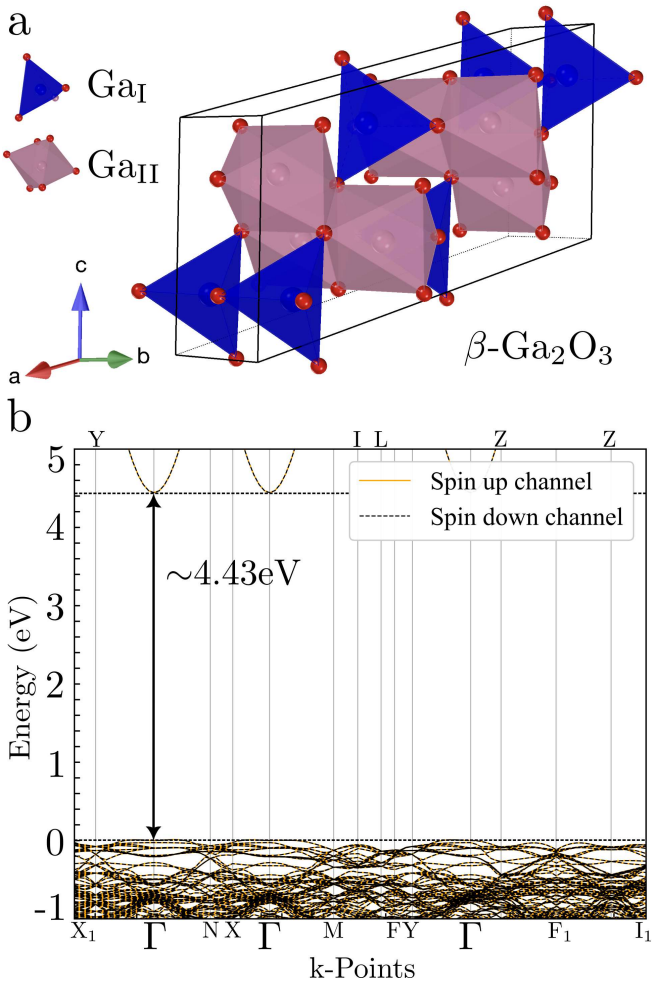

FIG. 1. (a) Crystal structure of monoclinic β-Ga_2O_3 (space group C2/m). The two inequivalent cation sites are highlighted: the tetrahedral, fourfold-coordinated Ga_I bonded to four oxygen atoms (blue), and the octahedral, sixfold-coordinated Ga_{II} bonded to six oxygen atoms (pink), red spheres denote O atoms. The 2×2×2 supercell used in the defect and self-trapped holes (STHs) calculations is obtained by replicating this conventional cell along the three crystallographic directions indicated by the axes. (b) Electronic band structure of pristine β-Ga_2O_3 calculated with the HSE hybrid functional using CRYSTAL23. The vertical arrow marks the calculated fundamental bandgap of 4.43 eV between the valence band maximum (VBM) and the conduction band minimum (CBM).

verge in showing that oxygen vacancies (VO) in β-Ga_2O_3 act as deep donors rather than the shallow electron sources once assumed. In the monoclinic lattice, VO can form on three inequivalent oxygen sites: O_I and O_{II} are threefold coordinated bonded to two Ga_{II} and one Ga_I (two Ga_I and one Ga_{II}), whereas O_{III} is fourfold coordinated bonded to three Ga_{II} and one Ga_I. This yields site-dependent local relaxations and charge-transition levels [16, 43, 44]. These vacancies substantially perturb the dielectric response and give rise to in-gap optical absorption as well as characteristic PL and CL bands [43–49], when present at high concentration. On the other hand, both types of possible gallium vacancies, VGa_I and VGa_{II}, act as deep acceptors and are the dominant compensating centers in n-type material, as shown by hybrid-DFT and EPR studies that directly resolve their ionized charge states. In β-Ga_2O_3, these defects correspond to the removal of Ga from either the tetrahedral or octahedral cation site, respectively, with each configuration exhibiting distinct local relaxations, defect levels and, in some cases, vacancy-induced magnetism [17, 46, 50–53].

Despite this progress, the connection between the local structure of Ga vacancies, the associated STH configurations, and their optoelectronic signatures is still incomplete. Model Hamiltonian studies of Holstein polarons have long stressed the importance of lattice relaxation pathways and phonon emission dynamics for nonequilibrium relaxation and recombination processes [54]. However, a similar level of microscopic detail is still missing for real defect structures in UWBG oxides. Most defect calculations treat vacancies and STHs separately, often in relatively small supercells, and focus on thermodynamic charge-transition levels or formation energies [28, 43, 55]. On the experimental side, CL and PL spectra exhibit numerous overlapping broad bands whose microscopic origin is difficult to disentangle. Only recently deep-UV emissions have been assigned specifically to Ga-vacancy related centers combining spectroscopy and first-principles modeling [23, 46].

In this work, we perform a detailed hybrid-DFT investigation of STHs associated with tetrahedral and octahedral gallium vacancies in bulk β-Ga_2O_3. Calculations are carried out using the CRYSTAL23 code [56] and a 2×2×2 supercell. We first benchmark the electronic structure of pristine β-Ga_2O_3, including the bandgap and band dispersion along its crystallographically k-path [6, 57–61]. We then introduce a gallium vacancy on the Ga_I and Ga_{II} sublattices and analyze the resulting defect states, local structural relaxations, and STH configurations for the relevant charge states [28, 62]. Particular attention is paid to how the local coordination and connectivity of the vacancy site control hole localization, spin-density distribution, and the position of in-gap defect levels. Finally, we discuss the consequences of these site-dependent STHs states for optical transitions in the UV-visible range, in light of existing PL, CL and XEOL data on β-Ga_2O_3, and outline some clues for future experiments [23, 31, 35, 36].

II. METHODS

All first-principles calculations were performed with the CRYSTAL23 toolkit [56], which solves the periodic Kohn–Sham equations using localized Gaussian-type orbital basis sets under full three-dimensional periodic boundary conditions. The electronic structure was treated within spin-polarized hybrid DFT using an HSE06 screened hybrid functional of the

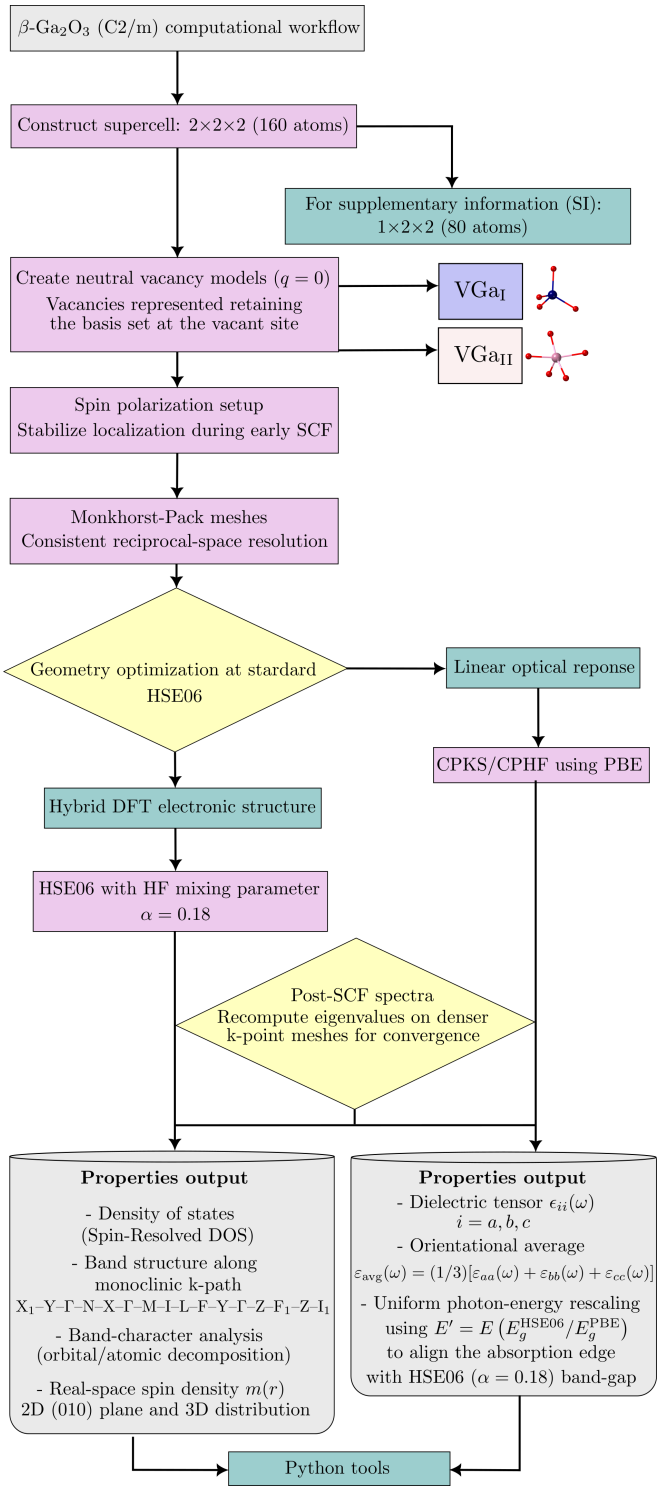

FIG. 2. Workflow for hybrid-DFT calculations of β-Ga_2O_3 with gallium vacancies. A $2\times2\times2$ (160-atom) supercell was used for the main results (with $1\times2\times2$ tests in the S.I.). Neutral vacancies VGa_I and VGa_{II} were modeled with a retained ghost basis at the vacant site and treated with spin-polarized HSE06 ($\alpha = 0.18$). Post-self-consistent-field properties were obtained on denser k meshes, while the dielectric response was computed with PBE-CPKS/CPHF and energy-rescaled to account for the more realistic HSE06 bandgap.

Heyd–Scuseria–Ernzerhof family [58, 63]. The standard screening parameter and fraction of exact exchange ($\alpha = 0.18$, i.e., 18% Hartree–Fock exchange) were chosen so that the bandgap of pristine β-Ga_2O_3 matches optical benchmarks and O-centered STH states are stabilized with realistic trapping energies [27–30, 59]. As shown in Fig. 1(b), the calculated band electronic structure of pristine β-Ga_2O_3 is that of a UWBG semiconductor yielding an energy band gap of $E_g = 4.43$ eV consistent with experimental values. We report the specific HSE06 parametrization used here, because the details of STHs stabilization and defect levels are known to be sensitive to the treatment of nonlocal (Hartree-Fock) exchange and screening of the Coulomb interaction in UWBG oxides. Our computational workflow is outlined in Fig. 2.

Band structure: supercell with neutral VGa

The host lattice is monoclinic β-Ga_2O_3 (space group C2/m). The primitive cell was fixed to the experimental lattice parameters $a = 12.215$ Å, $b = 3.050$ Å, $c = 5.820$ Å, and $\beta = 103.978°$, from which we built a $2\times2\times2$ supercell containing 160 atoms [7]. All results discussed in the main text are obtained for this supercell, which reduces periodic-image interactions and approximates the dilute-defect limit. A single vacancy in this supercell corresponds to one defect per 160 atoms (≈0.6 at.%) or per 64 gallium sites on the Ga sublattice. We considered both crystallographically distinct gallium vacancies, VGa_I on the tetrahedral sublattice and VGa_{II} on the octahedral sublattice, so that the resulting STHs can be correlated directly with the local Ga-O coordination. Additional tests using a smaller $1\times2\times2$ (80-atom) supercell are reported in the Supplementary Information. In these calculations, we explore higher nominal vacancy concentrations, oxygen vacancies, and vacancy-pair configurations to verify the robustness of the STH behavior identified in the dilute limit. Our results confirm that oxygen vacancies alone do not stabilize STHs under the considered conditions [43, 44, 46, 55].

All defect calculations were spin-polarized and performed without imposing symmetry constraints. Initial magnetic moments were placed on oxygen neighbors of the vacancy to seed hole localization. Then all internal coordinates were relaxed until residual atomic forces were negligible. This allows for the full development of the lattice spin-density associated with STH formation [28, 62]. Charged supercells were treated with a homogeneous compensating background; when formation energies or charge-transition levels are discussed, they follow the standard supercell formalism for point defects in solids [16, 43, 62]. The self-consistent-field (SCF) calculations employed a tight convergence criteria of 10^{-7} Hartree. Brillouin-zone sampling in the SCF calculations employed a Monkhorst-Pack mesh selected

to provide a consistent reciprocal-space resolution and k-point density across the supercells. Post-SCF properties were obtained by recomputing the eigenvalue spectrum on a denser k-point mesh to ensure convergence of spin-polarized results [64]. The supercells converged with respect to both the k-point sampling and the numerical integration thresholds, producing stable total energies.

Band structures were computed from the converged hybrid-DFT wavefunctions along a high-symmetry path for the monoclinic Brillouin zone X_1–Y–Γ–N–X–Γ–M–I–L–F–Y–Γ–Z–F_1–Z–I_1 following the convention of Peelaers and Van de Walle for β-Ga_2O_3 [57], which is compatible with more general crystallographic path definitions for low-symmetry lattices [60, 61]. Apparent bandgaps quoted in the figures are measured from the valence-band maximum (VBM) to the conduction-band minimum (CBM). For pristine β-Ga_2O_3, our HSE06 functional reproduces the experimental and previous theoretical bandgap range [6, 28, 48]. In defective cells, STH levels are identified by two complementary signatures: i) a magnetization density strongly localized on one (or a few) O ions neighboring the vacancy, and ii) nearly dispersionless flat bands within the gap. For each configuration we quantify the STH energy level as the energy separation between the VBM and the center of its corresponding flat band. Additionally the transition energy from the STHs level to the conduction band is taken as the separation between the latter and the CBM, according to previous studies on STHs acceptors in Ga_2O_3 [27, 29, 30, 39].

Spin-polarization in real and reciprocal space

In spin-polarized calculations it is important to distinguish two complementary representations. The α and β spin channels that appear in the density of states (DOS) and in the band structure describe the global spin-resolved Kohn-Sham spectrum of the full supercell. In this reciprocal-space representation, each eigenstate $\psi_{n\sigma}$ ($\sigma = \alpha$ or β) is labeled with the corresponding α or β spin channel. In contrast, the spatial distribution of the unpaired spin is revealed by the real-space magnetization (spin) density $m(\vec{r}) = \rho_\alpha(\vec{r}) - \rho_\beta(\vec{r})$, where $\rho_\sigma(\vec{r}) = \sum_n f_{n\sigma} \left|\psi_{n\sigma}(\vec{r})\right|^2$ is constructed from the spin-dependent Kohn-Sham orbitals and their occupations $f_{n\sigma}$ [65]. A compact measure of the same information can be obtained by integrating the spin densities within a chosen atomic basis (or projection region) associated with an atom i, which yields the spin-resolved populations N_i^σ and the corresponding local moment $m_i = N_i^\alpha - N_i^\beta$. A STH therefore appears in real space as a compact and anisotropic distribution of $m(\vec{r})$ (and an associate localized m_i) centered on a specific oxygen atom, even though the corresponding defect band can have weight in both α and β k-channels depending on hybridization and the symmetry of the local environment. This distinction matters because the $\alpha(\beta)$ channels describe the spin character of the eigenvalues in reciprocal space, while $m(\vec{r})$ and its site-dependent counterpart m_i identify the physical location of the localized state. In the STHs configurations studied here the magnetization is confined to one oxygen neighbor of the vacancy, accounting for a O-2p hole, and the spin-dependent flat defect band provide the reciprocal-space signature of the same localized state.

We quantify the relative stability of neutral gallium vacancies using the standard supercell formalism for point defects in solids [16, 43, 62]. For a vacancy on sublattice $\eta = \mathrm{I}$ or II, the formation energy is defined as $E_\mathrm{f}[\mathrm{VGa}_\eta] = E_\mathrm{tot}(\mathrm{VGa}_\eta) - E_\mathrm{tot}(\mathrm{Bulk}) + E^\mathrm{atom}_{\mathrm{Ga}_\eta}$, which, in the neutral charge state, reduces to the energetic cost of removing one Ga atom from the crystal and placing it into an atomic Ga reference (i.e., without Fermi-level–dependent terms or electrostatic image-charge corrections). With this convention, we obtain $E_\mathrm{f}(\mathrm{VGa_I}) = 10.37$ eV and $E_\mathrm{f}(\mathrm{VGa_{II}}) = 11.45$ eV, indicating that vacancy formation on the tetrahedral sublattice $\mathrm{VGa_I}$ is most favorable. Both the large formation energies (typically $\gtrsim 10$ eV) and the preference for the tetrahedral site are in line with prior hybrid-DFT calculations for isolated gallium vacancies in β-Ga_2O_3 [46, 66].

Real-space charge and spin densities were extracted on a dense real-space grid from the CRYSTAL23 wavefunctions. We employ two types of visualization: i) two-dimensional cuts of the spin-density in the (010) plane, which intersects both the tetrahedral and octahedral Ga-O chains, and ii) three-dimensional distributions of the real-space magnetization that make explicit the directional localization of the O-2p derived STHs. In the main text we focus on the dilute-defect 2×2×2 supercell to establish how the local coordination of the $\mathrm{VGa_I}$ and $\mathrm{VGa_{II}}$ sites controls the symmetry and energy of the associated STHs.

Linear optical response to a polarized electric field

To quantify how VGa and STH formation modify the linear optical response, we evaluated the purely electronic (clamped-ion) contribution to the dielectric tensor using the periodic coupled-perturbed Hartree-Fock/Kohn-Sham (CPHF/KS or CPKS) formalism as implemented in CRYSTAL23. Within this framework, the first-order response of the density matrix to a homogeneous external polarized electric field is obtained self-consistently by solving the CPKS equations in the occupied-virtual Bloch-orbital manifold. Here, the external field corresponds to the long-wavelength (optical) limit of a time-dependent perturbation, so that the electric field is taken as spatially uniform over the periodic cell and only the polarization direction and frequency of $\vec{E}(\omega)$ are specified. The resulting analytical second derivatives of the total energy with respect to the field yield the frequency-dependent dielectric tensor $\varepsilon(\omega)$ (and the associated linear susceptibilities), without considering finite-field effects [67–69]. Because the present CPKS implementation does not support hybrid functionals, the dielectric

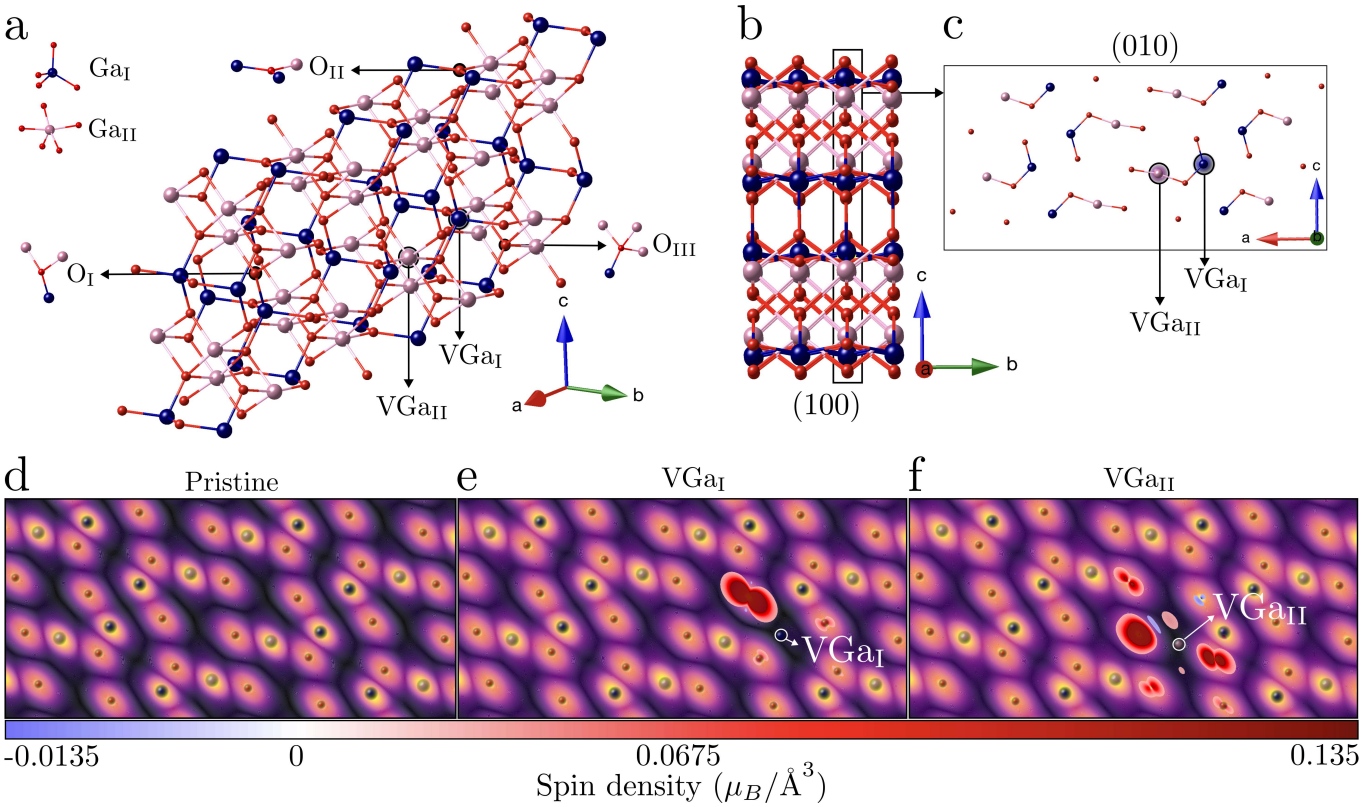

FIG. 3. Crystal structure and spin-density distribution of β-Ga_2O_3 with gallium vacancies. (a) $2 \times 2 \times 2$ β-Ga_2O_3 supercell indicating the two inequivalent Ga sites (tetrahedral Ga_I and octahedral Ga_{II}) and the three inequivalent O sites (O_I, O_{II} and O_{III}). The positions of Ga vacancies, VGa_I and VGa_{II}, are indicated. (b) Side view along the plane (100) that highlights the slab used for the spin-density analysis. (c) View of the (010) plane where VGa_I and VGa_{II} are introduced. (d-f) Spin-density maps on the (010) plane for β-Ga_2O_3 (d) pristine, (e) supercell with VGa_I, and (f) supercell with VGa_{II}. The color scale highlights the localization of the magnetic moment on O atoms neighboring the Ga vacancies, demonstrating the STH formation.

response was computed at the semilocal PBE level [70]. However we performed an energy rescaling at the end of process to account for a more realistic electronic structure. The Brillouin-zone sampling was kept identical to that used in the ground-state calculations.

Optical absorption spectra were obtained for a field-polarization parallel to one of the three relevant crystalographic axis, $\vec{E} \parallel \vec{a}$, $\vec{E} \parallel \vec{b}$, and $\vec{E} \parallel \vec{c}$, and the global optical response was defined as the following average $\varepsilon_{\rm avg}(\omega) = (1/3)[\varepsilon_{aa}(\omega) + \varepsilon_{bb}(\omega) + \varepsilon_{cc}(\omega)]$. For every polarization $j \in \vec{a}, \vec{b}, \vec{c}$, the corresponding dielectric response $\varepsilon_{jj}(\omega)$ was used to reconstruct the complex refractive index $\tilde{n}_j(\omega) = \sqrt{\varepsilon_{jj}(\omega)} = n_j(\omega) + ik_j(\omega)$. Last, the polarization-dependent absorption coefficient was then obtained as $\alpha_j(\lambda) = 4\pi k_j/\lambda$. It is worth noticing that, although PBE correctly captures the STHs lattice distortion, it underestimates the bandgap $E_g^{\rm PBE}$ of UWBG oxides. Therefore, to place the PBE-CPKS optical spectra on a consistent energy scale with the hybrid-DFT electronic structure, a scale factor $E_g^{\rm HSE}/E_g^{\rm PBE}$ was applied to the photon-energy axis so that the fundamental absorption edge coincides with the HSE06 bandgap $E_g^{\rm HSE}$.

III. RESULTS AND DISCUSSION

Our results reveal a one-to-one correspondence between vacancy sublattice (VGa_I or VGa_{II}), preferred oxygen-centered STH site (O_{II} or O_{III}), and polarization-selective near-edge optical transitions.

A. Electronic structure of vacancy-induced self-trapped holes

Figure 3 summarizes the structural motifs that control hole localization in β-Ga_2O_3 when a gallium vacancy is introduced. The $2 \times 2 \times 2$ supercell in Fig. 3(a) highlights the two inequivalent Ga sublattices, tetrahedral Ga_I and octahedral Ga_{II}, together with the three inequivalent oxygen sites O_I, O_{II}, and O_{III}. The introduction of a vacancy at either Ga site (VGa_I or VGa_{II}) removes a Ga-O coordination center and produces an acceptor-like perturbation in a lattice whose valence band is dominated by O-2p states. This situation is known to favor hole self-trapping localization in Ga_2O_3 [25, 26, 30].

Spin-density maps in Fig. 3(d-f), corresponding to

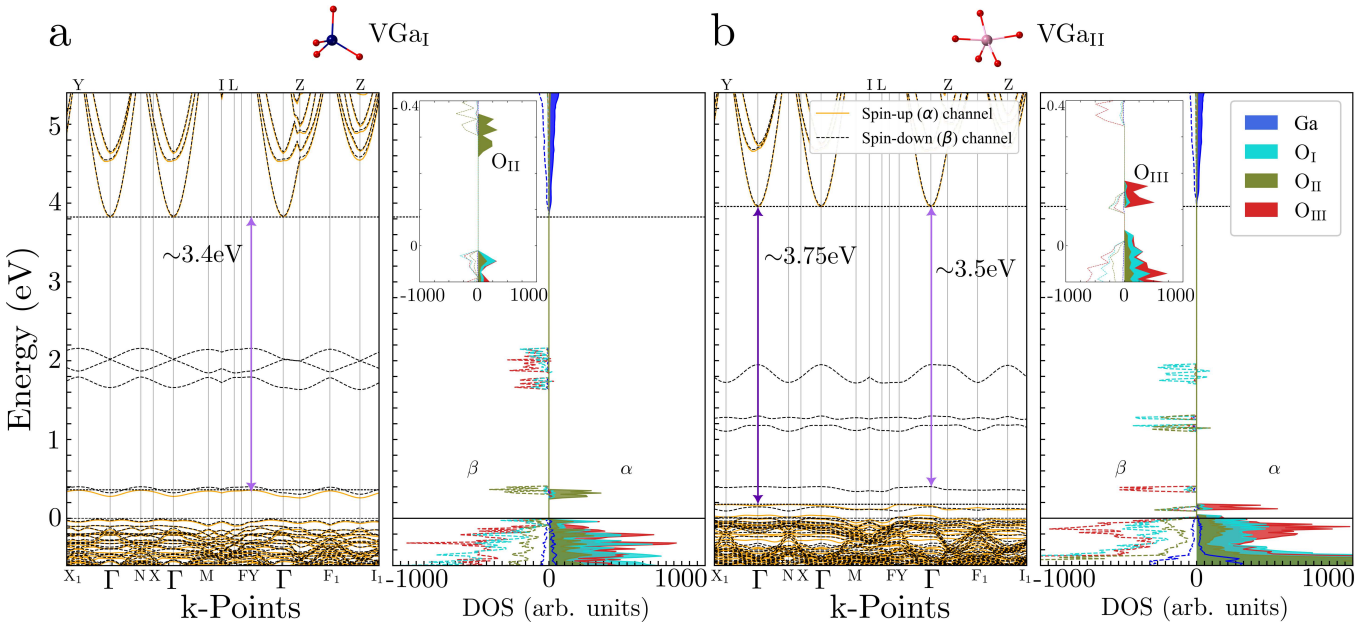

FIG. 4. spin-polarized band structures and projected densities of states (DOS) for fully relaxed β-Ga_2O_3 supercells containing (a) a tetrahedral VGa_I and (b) an octahedral VGa_{II}. Left panels show the spin-resolved band structure along the selected high-symmetry path with the VBM set to 0 eV and the CBM of pristine β-Ga_2O_3 indicated by the horizontal dashed line. The narrow in-gap band just above the VBM corresponds to the STH bound to the VGa that is strongly spin-polarized. This gives rise to optical transitions to the CBM of 3.4 eV for VGa_I and 3.75 eV/3.5 eV for VGa_{II}, as marked by the vertical arrows. Right panels display the atom and spin-resolved DOS, separated into α (spin-up) and β (spin-down) channels, with colors denoting contributions from Ga (blue), O_I (cyan), O_{II} (green), and O_{III} (red). Insets expand the energy window to highlight the character of the STHs in-gap state. Results show that it is dominated by O_{II} character for VGa_I and by O_{III} character for VGa_{II}.

the (010) plane cut indicated in Fig. 3(b,c), provide direct real-space evidence for vacancy-bound hole localization. The pristine supercell Fig. 3(d) is essentially nonmagnetic on this scale, whereas both supercells containing vacancies develop a highly localized spin-density on oxygen neighbors of the missing Ga, see Fig. 3(e,f). This localization is the defining signature of a trapped hole bound to the vacancy, rather than a delocalized valence-band hole. We find that the magnetization concentrates on specific O sites adjacent to VGa_I and VGa_{II}, consistent with prior understanding that Ga vacancies in β-Ga_2O_3 act as compensating acceptors and hole traps [72–74]. This is also in agreement with the experimental identification of vacancy-related paramagnetic centers, where the unpaired spin is predominantly oxygen-centered [50]. Crucially for our analysis, the (010)-plane maps already indicate site-selective STH formation: VGa_I and VGa_{II} localize the hole on distinctly different oxygen sublattices.

Results shown in Fig. 4 links the real-space localization to the electronic structure of the material. For supercells with VGa_I [Fig. 4(a)] or VGa_{II} [Fig. 4(b)], the spin-polarized band structures show a narrow, strongly spin-polarized in-gap band just above the VBM. This spectrally isolated band near the top of the valence manifold corresponds to a vacancy-bound STH that is spatially localized, as illustrated in Fig. 3. The flat in-gap band together with the localized O-centered spin-density provides complementary reciprocal- and real-space fingerprints of a vacancy-bound STH.

To identify the atomic origin of the vacancy-induced in-gap bands, we analyzed the dominant components of the crystalline-orbital eigenvectors together with the atom-projected DOS. In both defective supercells, the states appearing inside the pristine bandgap are clearly related to oxygen orbitals with a clear 2p character. This confirms that the VGa binds to oxygen-centered trapped-hole states rather than creating Ga-centered defect levels. Importantly, the oxygen sublattice hosting the in-gap state depends on the vacancy site: for the tetrahedral gallium vacancy VGa_I, the highest-lying in-gap eigenvectors are dominated by O_{II} contributions, while for the octahedral vacancy VGa_{II} the corresponding in-gap states are dominated by O_{III} contributions. We also find a smaller additional localized in-gap contributions with O_I character in both configurations. This is consistent with reports of multiple stable oxygen-centered trapped-hole configurations from hybrid-DFT studies, as well as with EPR and theoretical assignments of Ga-vacancy-related paramagnetic centers in β-Ga_2O_3 [27–30, 51, 52].

Remarkably for optical properties, the vacancy-bound STH introduces a new excitation transition, from the in-gap state to the CBM. The vertical arrows in Fig. 4 show the corresponding transition energies: 3.4 eV for VGa_I, 3.75 eV and 3.5 eV for VGa_{II}. These values fall in the

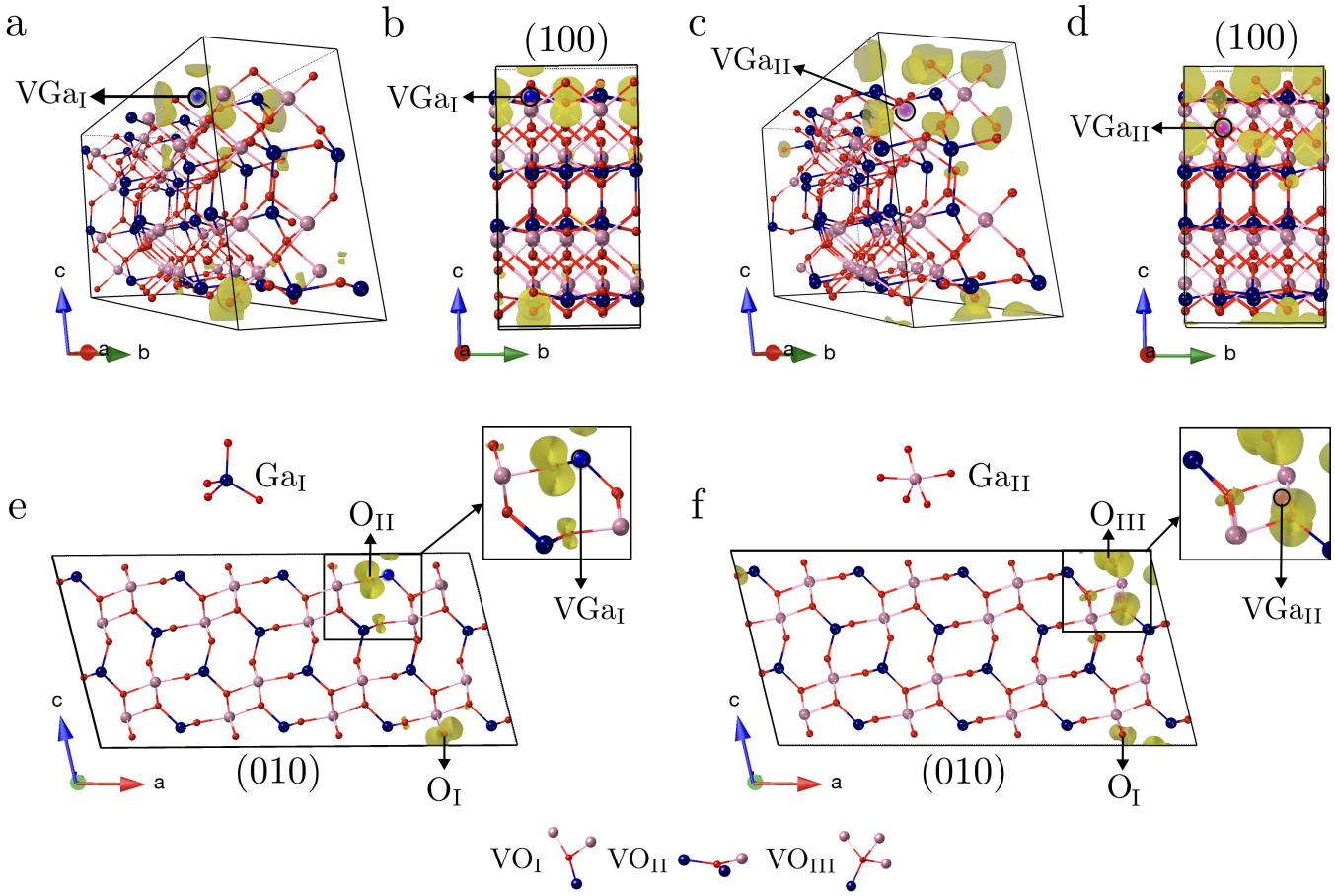

FIG. 5. Fully relaxed atomic structures and spin-density distributions showing STHs bound to VGa in β-Ga_2O_3. Panels (a,b) display the geometry-optimized supercell containing tetrahedral VGa_I in 3D perspective and along the (100) plane, respectively. Panels (c,d) show the corresponding views for the octahedral VGa_{II}. Yellow distributions represent the spin-density of the trapped hole, illustrating its strong localization on O neighbors to the VGa and the associated lattice distortion. Panels (e,f) show the relaxed (010) slabs around VGa_I and VGa_{II} respectively, with insets highlighting the local environments of the STHs centered on O_{II} in (e) and on O_{III} in (f). These configurations correspond to O_{II} and O_{III} centered STHs. Both reveals a reduced additional O_I STHs contributions as expected [71]. The relative displacement of the atoms surrounding the VGa proves the structural relaxation that accompanies STH formation. Ga_I, Ga_{II}, and O atoms are shown in blue, pink and red, respectively.

same energy window as the polarization-dependent deep-UV and UV luminescence bands reported in polarization-resolved XEOL on β-Ga_2O_3 membranes [23]. The optical transitions allowed by the new vacancy-bound states will be studied within the absorption spectra calculated with CRYSTAL23 below.

Figure 5 provides the direct atomistic picture behind the electronic fingerprints of Fig. 4. The optimized geometries show that introducing either VGa_I or VGa_{II} triggers a localized structural relaxation around the vacancy. Indeed, the yellow spin-density distributions demonstrate that the trapped hole is not distributed uniformly over all oxygen neighbors. Instead, it condenses into a STHs centered on a specific oxygen sublattice; O_{II} for VGa_I [Fig. 5(e)] and O_{III} for VGa_{II} [Fig. 5(f)], with additional O_I STHs appearing as accompanying localized holes. This combination of electronic localization and local lattice distortion is precisely what is expected for a STH stabilized by strong electron–phonon coupling in an ultrawide bandgap oxide [25, 26, 54].

There are two key takeaways from Fig. 5. First, the vacancy type determines which oxygen sublattice participates in hole trapping. This explains the dominance of O_{II} versus O_{III} character of the in-gap states observed in the DOS insets shown in Fig. 4(a) and (b), respectively. Second, because the trapped-hole wavefunction is O-2p like and particularly oriented by the local bonding environment, VGa_I and VGa_{II} bound STHs are expected to give a different optical response. Thus, the optical transitions mediated by the vacancy-induced bound states will depend on the particular direction of the electric field polarization. The latter leads to a microscopic explanation of the polarization effects observed in recent XEOL experiments [23]. Our results on real-space state localiza-

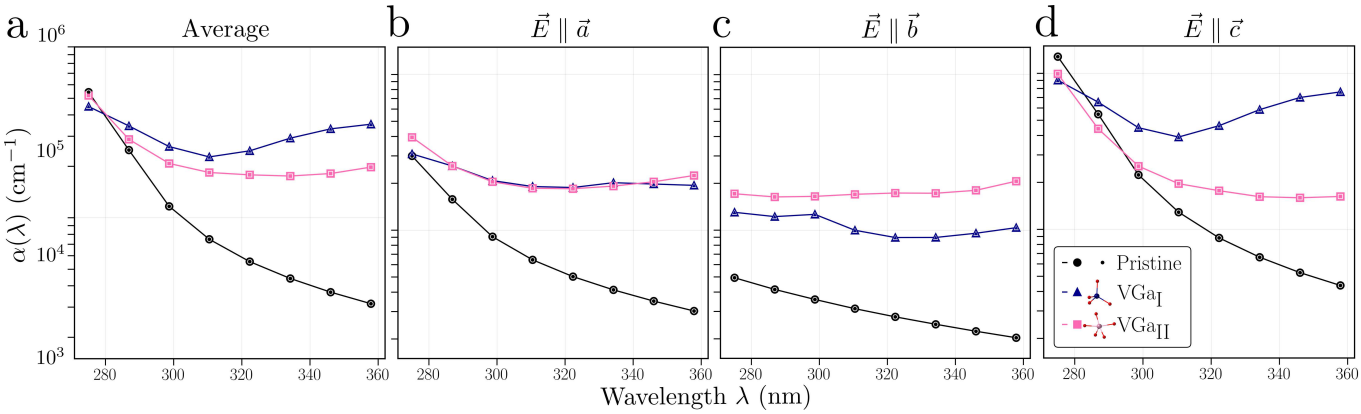

FIG. 6. Polarization-dependent absorption coefficient $\alpha(\lambda)$ of β-Ga2O3 and Ga-vacancy supercells. Spectra are shown for pristine β-Ga2O3 (black circles) and for fully relaxed supercells containing either a tetrahedral VGaI (blue triangles) or an octahedral VGaII (pink squares). Panel (a) shows the averaged absorption, defined as the arithmetic mean of the absorption coefficients computed for incident electric-field-polarization along the monoclinic crystallographic axes, $\varepsilon_{\mathrm{avg}}(\omega) = (1/3)\,[\varepsilon_{aa}(\omega) + \varepsilon_{bb}(\omega) + \varepsilon_{cc}(\omega)]$, and panels (b–d) resolve the absorption for incident electric-field-polarization along the monoclinic $\vec{a}$, $\vec{b}$, and $\vec{c}$ axes, respectively. To compensate for the bandgap underestimation at the PBE level, the photon-energy axis was uniformly rescaled according to $E' = E\ (E_g^{\mathrm{HSE06}}/E_g^{\mathrm{PBE}})$, with the wavelength axis updated consistently with $\lambda' = hc/E'$. The vacancy-induced optical response is anisotropic and depends strongly on the inequivalent vacancy site. For $\vec{E} \parallel \vec{b}$, the VGa$_{\mathrm{II}}$ center consistently exhibits higher absorption than VGa$_{\mathrm{I}}$ over the explored wavelength range. In contrast, for $\vec{E} \parallel \vec{c}$, the absorption associated with VGa$_{\mathrm{I}}$ becomes dominant at longer wavelengths. Absorption is plotted on a logarithmic ordinate with identical y-axis limits in all panels to enable direct comparison of absolute magnitudes across polarizations and defect types.

tion and electronic band structure not only show how gallium vacancies stabilize oxygen-centered STHs, but also demonstrate that inequivalent VGa give rise to distinct STH centers with different near-UV optical transition energies [71].

B. Linear optical response

To establish a direct link between vacancy-induced STHs and experimentally accessible electric-field-polarization signatures, we computed the linear absorption coefficient from the imaginary part of the electronic (clamped-ion) dielectric tensor within the CPHF/KS framework as implemented in CRYSTAL23 [56, 67–69]. Because $\varepsilon(\omega)$ is evaluated in the long-wavelength optical limit, the computed anisotropy is controlled by the orientation of the incident electric-field vector $\vec{E}$ with respect to the crystallographic axes, while the explicit propagation direction of the electromagnetic wave is not considered. In monoclinic β-Ga_2O_3, the dielectric tensor is, in general, not strictly diagonal in the crystallographic basis, and symmetry allows nonzero off-diagonal components [4, 20, 75]. In this work we present polarization-resolved spectra for incident fields aligned along the crystallographic axes, $\vec{E} \parallel \vec{a}$, $\vec{E} \parallel \vec{b}$, and $\vec{E} \parallel \vec{c}$, and we therefore frame the discussion in terms of ε_{aa}, ε_{bb}, and ε_{cc}. The off-diagonal components obtained in our calculations are small in the wavelength window considered here, so including them would not remarkably change the trends discussed below [75]. Full-tensor optical analyses that explicitly include the off-diagonal components have also been reported [76]. The pristine lattice already exhibits a pronounced monoclinic optical anisotropy and an electric-field polarization dependent near-edge response. It is worth to mention that the absorption edge of different polarized spectra (reflectance, electroreflectance and transmittance) has been demonstrated to be lower in energy when $\vec{E} \parallel \vec{a}$ or $\vec{E} \parallel \vec{c}$ than for the case $\vec{E} \parallel \vec{b}$. In addition those experiments have revealed a substantially stronger near-edge absorption for $\vec{E} \parallel \vec{c}$ than for $\vec{E} \parallel \vec{b}$ [4, 19–22, 77]. This experimental trend agrees with our absorption spectra for the pristine lattice shown in Fig. 6(b-d), where the $\vec{E} \parallel \vec{b}$ response is markedly suppressed over the displayed wavelength window compared to that of $\vec{E} \parallel \vec{a}$ and $\vec{E} \parallel \vec{c}$.

The introduction of gallium vacancies enhances the near-edge absorption tail and, importantly, produces a clear vacancy-selective dichroism associated with the inequivalent tetrahedral and octahedral gallium sublattices (VGa$_{\mathrm{I}}$ vs VGa$_{\mathrm{II}}$) [16, 50–52, 72–74]. For a field with polarization $\vec{E} \parallel \vec{b}$, the absorption spectra in Fig. 6(c) show that the lattice with octahedral vacancies VGa$_{\mathrm{II}}$ consistently exhibits stronger absorption than the one with the tetrahedral vacancy VGa$_{\mathrm{I}}$ across the entire spectral window considered. In contrast, when the field polarization is $\vec{E} \parallel \vec{c}$, Fig. 6(d) reveals a reversal of this trend at longer wavelengths, where the absorption of the lattice

with VGa_I exceeds that of the lattice with VGa_{II}. However no similar signatures are present when $\vec{E} \parallel \vec{a}$, see Fig. 6(b). Therefore, the calculated absorption reveals a vacancy-selective dichroism: the absorption of lattices with VGa_{II} is dominated by polarization fields such as $\vec{E} \parallel \vec{b}$. On the contrary, if VGa_I are present in the system, it is the polarization $\vec{E} \parallel \vec{c}$ that provides a stronger absorption.

In our microscopic picture, the linear dichroism originates from the O-2p character of the vacancy-bound hole. The corresponding STH is pinned by the local Ga-O connectivity, which differs for tetrahedral and octahedral vacancy sites. This local geometry fixes the orientation of the wavefunction and, as a result, the relevant components of the dipole moments involved in the optical transitions between the STH state and the CBM. Therefore, this yields different oscillator strengths for different polarizations of the electric field, $\vec{E} \parallel \vec{b}$ or $\vec{E} \parallel \vec{c}$ [25–28, 30]. The resulting polarization selectivity is consistent with the site-resolved XANES-XEOL measurements where the UV transition is more strongly affected by VGa_I environments, while the deep-UV and blue spectral bands are enhanced in the presence of VGa_{II} network [23, 33, 78].

Although XEOL probes radiative recombination rather than optical absorption, for a given electronic transition the absorption coefficient and the radiative emission rate are governed by the same electric-dipole matrix elements. Thus absorption and emission share the polarization selection rules [79–81]. In the quasi-equilibrium limit (often used as a working approximation for luminescence analysis), reciprocity and detailed-balance arguments further relate the spontaneous-emission spectrum to the absorption coefficient [82–84]. For low-symmetry crystals these relations apply mode-by-mode, so the connection holds separately for each polarization component of the optical response tensor. Accordingly, we use the DFT-computed dichroism of $\alpha(\omega)$ primarily as a proxy for the polarization dependence of the underlying radiative dipole channel, while noting that absolute XEOL intensities additionally depend on non-equilibrium carrier populations, capture kinetics, and optical outcoupling.

IV. CONCLUSIONS

In this work we combined spin-polarized hybrid DFT with first-principles optical-response calculations to establish a microscopic link between gallium vacancies, vacancy-bound hole self-trapping, and electric field polarization selective near-edge optical absorption in monoclinic β-Ga_2O_3. By explicitly treating vacancies on the two inequivalent Ga sublattices (tetrahedral Ga_I and octahedral Ga_{II}) within a dilute-defect $2\times2\times2$ supercell, we show that the local Ga–O coordination controls both the stability and the electronic fingerprint of vacancy STHs complexes. In both vacancy configurations the unpaired hole localizes on specific oxygen neighbors, producing an oxygen-centered STH rather than a delocalized valence-band hole. Importantly, the preferred oxygen sublattice is vacancy-site dependent: VGa_I stabilizes primarily an O_{II}-centered STH, whereas VGa_{II} favors a distinct configuration dominated by O_{III} character. These results identify VGa_I and VGa_{II} STHs complexes as inequivalent microscopic centers despite their identical chemical stoichiometry.

In reciprocal space, the vacancy-bound STHs manifest as narrow, weakly dispersive, spin-polarized states near the top of the valence manifold, enabling defect-specific optical transitions to the conduction-band edge. Within the present framework, these transitions appear in the near-UV/deep-UV energy window, consistent with the spectral range where Ga-vacancy-related luminescence features have been reported [23, 38, 49]. We stress that absolute transition energies and intensities can be affected by effects not explicitly captured here (e.g., excitonic corrections, vibronic broadening, finite-temperature carrier populations, and the non-equilibrium kinetics inherent to XEOL). Our goal is therefore not a quantitative comparison with previous experiments, but a first-principle identification of how defect symmetry and STHs real-space structure constrain the allowed optical dipole transitions.

A central prediction of this study is a vacancy-dependent linear dichroism in the near-edge absorption: field-polarization-resolved spectra show that VGa_{II} enhances absorption for $\vec{E} \parallel \vec{b}$, whereas VGa_I dominates for the absorption for $\vec{E} \parallel \vec{c}$, with differences reaching several-fold at long wavelengths. Because polarization selection rules are shared by absorption and radiative emission, we provide a physically motivated basis for qualitative comparison with polarization-resolved luminescence (PL, CL or XEOL) and suggests testable signatures for distinguishing vacancy populations in low-symmetry β-Ga_2O_3. On a broader scope, our results highlight vacancy-STHs complexes as distinct active centers that should be treated explicitly when interpreting optical anisotropy, and defect-controlled functionalities in ultrawide bandgap oxides. The explicit consideration of excitonic effects and excited-state relaxation is beyond the scope of this work but it would be required for a future quantitative emission modeling.

DECLARATIONS

Author Contributions

F.B.-M., E.D. and R.M.-C. wrote the manuscript. F.B.-M. prepared the figures. F.B.-M., E.D., B.M., E.N., F.D.-A. and R.M.-C. contributed to the scientific discussion prior to manuscript preparation and revised the manuscript.

Competing Interests

The authors declare no competing interests.

ACKNOWLEDGMENTS

This work was supported by the "(MAD2D-CM)-UCM" project funded by Comunidad de Madrid, by the Recovery, Transformation and Resilience Plan, and European Union NextGenerationEU/PRTR. The authors also acknowledge funding from Agencia Estatal de Investigación of Spain (MCIN/AEI/10.13039/501100011033) through Grants PCI2023-143388, PID2021-122562-NB-I00, PID2022-136285NB-C31 and PID2024-155966-NB-I00.

[1] M. H. Wong, O. Bierwagen, R. J. Kaplar, *et al.*, Ultrawide-bandgap semiconductors: An overview, J. Mater. Res. **36**, 4601 (2021).

[2] S. J. Pearton, J. Yang, P. H. Cary, F. Ren, J. Kim, M. J. Tadjer, and M. A. Mastro, A review of Ga_2O_3 materials, processing, and devices, Appl. Phys. Rev. **5**, 011301 (2018).

[3] Z. Galazka, Growth of bulk β-Ga_2O_3 single crystals by the czochralski method: A tutorial, J. Appl. Phys. **131**, 031103 (2022).

[4] F. Ricci, F. Boschi, A. Baraldi, A. Filippetti, M. Higashiwaki, A. Kuramata, V. Fiorentini, and R. Fornari, Theoretical and experimental investigation of optical absorption anisotropy in β-Ga_2O_3, J. Phys.: Condens. Matter **28**, 224005 (2016).

[5] N. Ueda, H. Hosono, R. Waseda, and H. Kawazoe, Synthesis and control of conductivity of ultraviolet transmitting β-Ga_2O_3 single crystals, Appl. Phys. Lett. **70**, 3561 (1997).

[6] M. Mohamed, C. Janowitz, I. Unger, R. Manzke, Z. Galazka, R. Uecker, R. Fornari, J. R. Weber, J. B. Varley, and C. G. Van de Walle, The electronic structure of β-Ga_2O_3, Appl. Phys. Lett. **97**, 211903 (2010).

[7] J. Åhman, G. Svensson, and J. Albertsson, A reinvestigation of β-gallium oxide, Acta Crystallogr., Sect. C: Cryst. Struct. Commun. **52**, 1336 (1996).

[8] E. Farzana, Z. Zhang, P. K. Paul, A. R. Arehart, and S. A. Ringel, Influence of metal choice on (010) β-Ga_2O_3 schottky diode properties, Appl. Phys. Lett. **110**, 202102 (2017).

[9] M. Higashiwaki, K. Sasaki, A. Kuramata, T. Masui, and S. Yamakoshi, Gallium oxide (Ga_2O_3) metal-semiconductor field-effect transistors on single-crystal β-Ga_2O_3 (010) substrates, Appl. Phys. Lett. **100**, 013504 (2012).

[10] M. Higashiwaki, K. Sasaki, T. Kamimura, M. H. Wong, D. Krishnamurthy, A. Kuramata, T. Masui, and S. Yamakoshi, Depletion-mode Ga_2O_3 metal-oxide-semiconductor field-effect transistors on β-Ga_2O_3 (010) substrates and temperature dependence of their device characteristics, Appl. Phys. Lett. **103**, 123511 (2013).

[11] J. Blevins and G. Yang, On optical properties and scintillation performance of emerging Ga_2O_3: Crystal growth, emission mechanisms and doping strategies, Mater. Res. Bull. **144**, 111494 (2021).

[12] X. Chen, F. Ren, S. Gu, and J. Ye, Review of gallium-oxide-based solar-blind ultraviolet photodetectors, Photonics Res. **7**, 381 (2019).

[13] M. Li, Y. Chen, C. Zhang, S. Khan, Z. Ke, S. Ding, Y. Wang, X. Xu, *et al.*, High-performance β-Ga_2O_3 schottky barrier diodes with Mg current blocking layer using spin-on-glass technique, Appl. Phys. Lett. **125**, 132101 (2024).

[14] C. Bouhafs, D. Carrasco, R. Lorena, C. Alfisi, J. Dolado, P. Pérez-Peinado, P. Hidalgo, D. Caetano, G. Martínez-Criado, B. Méndez, E. Nogales, K. Lorenz, and S. Cardoso, Self-powered uvc and X-Ray photodetection in single Sn-Doped β-Ga_2O_3 microwire schottky diodes, Adv. Mater. Technol. **10**, e01212 (2025).

[15] M. Mohamed, I. Unger, C. Janowitz, R. Manzke, Z. Galazka, R. Uecker, and R. Fornari, The surface band structure of β-Ga_2O_3, J. Phys.: Conf. Ser. **286**, 012027 (2011).

[16] M. D. McCluskey, Point defects in Ga_2O_3, J. Appl. Phys. **127**, 101101 (2020).

[17] X. He, H. Yan, Q. Yu, L. Ma, Z. Guo, and F. Liu, The effect of vacancy defects on the electronic properties of β-Ga_2O_3, Comput. Mater. Sci. **215**, 111777 (2022).

[18] V. Patil, B.-T. Lee, and S.-H. Jeong, Optical and structural characterization of high crystalline β-Ga_2O_3 films prepared using an rf magnetron sputtering, J. Alloys Compd. **894**, 162551 (2022).

[19] M. Yamaga *et al.*, Polarization of optical spectra in transparent conductive oxide β-Ga_2O_3, Phys. Status Solidi C **8**, 2621 (2011).

[20] M. Schubert, R. Korlacki, S. Knight, *et al.*, Anisotropy, phonon modes, and free charge carrier parameters in monoclinic β-gallium oxide single crystals, Phys. Rev. B **93**, 125209 (2016).

[21] P. Gopalan, S. Knight, A. Chanana, M. Stokey, P. Ranga, M. A. Scarpulla, S. Krishnamoorthy, V. Darakchieva, Z. Galazka, K. Irmscher, A. Fiedler, S. Blair, M. Schubert, and B. Sensale-Rodriguez, Optical anisotropy of (010) β-Ga_2O_3, Appl. Phys. Lett. **117**, 252103 (2020).

[22] M. M. R. Adnan, D. Verma, C. Sturm, M. Schubert, and R. C. Myers, The anisotropic beer–lambert law in β-Ga_2O_3: Spectral and polarization dependent absorption and photoresponsivity, Phys. Rev. Applied **21**, 054059 (2024).

[23] P. Pérez-Peinado, J. Dolado, P. L. Alcázar Ruano, D. Carrasco, R. Martínez-Casado, V. Bonino, G. Martínez-Criado, J. Jesenovec, J. S. McCloy, F. Domínguez-Adame, J. Quereda, E. Nogales, and B. Méndez, Proving optical anisotropy and polarization effects in β-Ga_2O_3 nanomembranes via x-ray excited optical luminescence, Adv. Photon. Res. **6**, 2000043 (2025).

[24] S. I. Pekar, Local quantum states of an electron in an ideal ionic crystal, Zh. Eksp. Teor. Fiz. **16**, 341 (1946).

[25] B. E. Kananen, N. C. Giles, L. E. Halliburton, G. K. Foundos, K. B. Chang, and K. T. Stevens, Self-trapped holes in β-Ga_2O_3 crystals, J. Appl. Phys. **122**, 215703 (2017).

[26] Y. K. Frodason, K. M. Johansen, L. Vines, and J. B. Varley, Self-trapped hole and impurity-related broad luminescence in β-Ga_2O_3, J. Appl. Phys. **127**, 075701 (2020).

[27] T. Gake, Y. Kumagai, and F. Oba, First-principles study of self-trapped holes and acceptor impurities in polymorphs of Ga_2O_3, Phys. Rev. Mater. **3**, 044603 (2019).

[28] P. Deák, Q. D. Ho, F. Seemann, B. Aradi, M. Lorke, and T. Frauenheim, Choosing the correct hybrid for defect calculations: A case study on intrinsic carrier trapping in β-Ga_2O_3, Phys. Rev. B **95**, 075208 (2017).

[29] C. Kaewmeechai, J. Strand, and A. L. Shluger, Electronic structure and properties of trapped holes in crystalline and amorphous Ga_2O_3, Phys. Rev. B **111**, 035203 (2025).

[30] J. L. Lyons, Self-trapped holes and polaronic acceptors in ultrawide-bandgap oxides, J. Appl. Phys. **131**, 025701 (2022).

[31] J. Huso, M. D. McCluskey, Y. Yu, M. M. Islam, and F. Selim, Localized uv emitters on the surface of β-Ga_2O_3, Sci. Rep. **10**, 21022 (2020).

[32] L. Binet and D. Gourier, Origin of the blue luminescence of β-Ga_2O_3, J. Phys. Chem. Solids **59**, 1241 (1998).

[33] Q. D. Ho, T. Frauenheim, and P. Deák, Origin of photoluminescence in β-Ga_2O_3, Phys. Rev. B **97**, 115163 (2018).

[34] H. Liu, C. Xu, X. Pan, and Z. Ye, The photoluminescence properties of β-Ga_2O_3 thin films, J. Electron. Mater. **49**, 4544 (2020).

[35] E. Nogales, B. Méndez, and J. Piqueras, Cathodoluminescence from β-Ga_2O_3 nanowires, Appl. Phys. Lett. **86**, 113112 (2005).

[36] A. Khan, W. M. Jadwisienczak, H. J. Lozykowski, and M. E. Kordesch, Fabrication and luminescence properties of monoclinic gallium oxide (β-Ga_2O_3) nanostructures, in *Materials Research Society Symposium Proceedings*, Vol. 951 (Materials Research Society, 2007) pp. E09–42.

[37] F. Matar, Y.-L. Shi, F. C.-C. Ling, A. Salih, C. P. Irvine, S. De Silva, M. R. Phillips, and C. Ton-That, Bandgap narrowing and hole self-trapping reduction in Ga_2O_3 by bi_2o_3 alloying, J. Alloys Compd. **960**, 170983 (2023).

[38] N. Hajizadeh, Y. K. Frodason, C. Petersen, B. M. Janzen, L. S.-M. Choi, N. Bernhardt, F. Nippert, Z. Galazka, J. B. Varley, H. von Wenckstern, L. Vines, and M. R. Wagner, Self-trapped hole migration and defect-mediated thermal quenching of luminescence in α- and β-Ga_2O_3, Adv. Funct. Mater. **36**, 202517876 (2025).

[39] J. L. Lyons, A survey of acceptor dopants for β-Ga_2O_3, Semicond. Sci. Technol. **33**, 05LT02 (2018).

[40] B.-S. Liao, M. Jung, J.-H. Seo, *et al.*, Exploration of p-type conductivity in β-Ga_2O_3 via Se–Mg codoping: a first-principles study, Mater. Today Adv. **18**, 100529 (2025).

[41] J. Liu, X. Xu, X. Xu, T. Ying, J. Yang, W. Li, and X. Li, Hybrid functional study of acceptor levels in β-Ga_2O_3 with stress engineering, J. Appl. Phys. **137**, 235703 (2025).

[42] M. Yamaga, H. Tsuzuki, S. Takano, E. G. Villora, and K. Shimamura, Electron-spin resonance of transparent conductive oxide β-Ga_2O_3, J. Non-Cryst. Solids **358**, 2458 (2012).

[43] T. Zacherle, P. C. Schmidt, and M. Martin, Ab initio calculations on the defect structure of β-Ga_2O_3, Phys. Rev. B **87**, 235206 (2013).

[44] J. B. Varley, J. R. Weber, A. Janotti, and C. G. Van de Walle, Oxygen vacancies and donor impurities in β-Ga_2O_3, Appl. Phys. Lett. **97**, 142106 (2010).

[45] H. Peelaers and C. G. Van de Walle, Sub-band-gap absorption in Ga_2O_3, Appl. Phys. Lett. **111**, 182104 (2017).

[46] A. Usseinov, Z. Koishybayeva, A. Platonenko, V. Pankratov, Y. Suchikova, A. Akilbekov, M. Zdorovets, J. Purans, and A. I. Popov, Vacancy defects in Ga_2O_3: First-principles calculations of electronic structure, Materials **14**, 7384 (2021).

[47] H. Dong, G. Yang, X. Fan, *et al.*, Effects of oxygen vacancies on structural and optical properties of β-Ga_2O_3, Sci. Rep. **7**, 40160 (2017).

[48] L. Y. Hao, J. L. Du, and E. G. Fu, Theoretical study on structural and optical properties of β-Ga_2O_3 with o vacancies via shell DFT-1/2 method, J. Appl. Phys. **134**, 085101 (2023).

[49] G. Pozina, M. Forsberg, M. A. Kaliteevski, and C. Hemmingsson, Emission properties of Ga_2O_3 nano-flakes: effect of excitation density, Sci. Rep. **7**, 42132 (2017).

[50] B. E. Kananen, N. C. Giles, L. E. Halliburton, G. Foundos, K. Chang, and K. T. Stevens, Gallium vacancies in β-Ga_2O_3 crystals, Appl. Phys. Lett. **110**, 202104 (2017).

[51] D. Skachkov, W. R. L. Lambrecht, H. J. von Bardeleben, U. Gerstmann, Q. D. Ho, and P. Deák, Computational identification of Ga-vacancy related electron paramagnetic resonance centers in β-Ga_2O_3, J. Appl. Phys. **125**, 185701 (2019).

[52] N. T. Son, Q. D. Ho, K. Goto, H. Abe, T. Ohshima, B. Monemar, Y. Kumagai, T. Frauenheim, and P. Deák, Electron paramagnetic resonance and theoretical study of gallium vacancy in β-Ga_2O_3, Appl. Phys. Lett. **117**, 032101 (2020).

[53] Y. Yang, J. Zhang, S. Hu, Y. Wu, *et al.*, First-principles study of ga-vacancy induced magnetism in β-Ga_2O_3, Phys. Chem. Chem. Phys. **19**, 28928 (2017).

[54] A. S. Mishchenko, N. Nagaosa, G. De Filippis, A. de Candia, V. Cataudella, N. V. Prokof'ev, A. Sakamoto, and B. V. Svistunov, Relaxation dynamics of the Holstein polaron, Phys. Rev. Lett. **109**, 236402 (2012).

[55] A. Usseinov, Z. Koishybayeva, A. Platonenko, *et al.*, First-principles study of defect pairs and vacancy complexes in β-Ga_2O_3, Opt. Mater. X **16**, 100200 (2022).

[56] A. Erba, J.-K. Desmarais, S. Casassa, B. Civalleri, L. Donà, I. J. Bush, B. Searle, L. Maschio, L.-E. Daga, A. Cossard, C. Ribaldone, E. Ascrizzi, N. L. Marana, J.-P. Flament, and B. Kirtman, CRYSTAL23: A program for computational solid state physics and chemistry, J. Chem. Theory Comput. **19**, 6891 (2023).

[57] H. Peelaers and C. G. Van de Walle, Brillouin zone and band structure of β-Ga_2O_3, Phys. Status Solidi B **252**, 828 (2015).

[58] J. Heyd, G. E. Scuseria, and M. Ernzerhof, Erratum: "hybrid functionals based on a screened coulomb potential" [j. chem. phys. 118, 8207 (2003)], J. Chem. Phys. **124**, 219906 (2006).

[59] A. V. Krukau, O. A. Vydrov, A. F. Izmaylov, and G. E. Scuseria, Influence of the exchange screening parameter on the performance of screened hybrid functionals, J. Chem. Phys. **125**, 224106 (2006).

[60] Y. Hinuma, G. Pizzi, Y. Kumagai, F. Oba, and I. Tanaka, Band structure diagram paths based on crystallography, Comput. Mater. Sci. **128**, 140 (2017).

[61] W. Setyawan and S. Curtarolo, High-throughput electronic band structure calculations: challenges and tools, Comput. Mater. Sci. **49**, 299 (2010).

[62] C. Freysoldt, J. Neugebauer, and C. G. Van de Walle, First-principles calculations for point defects in solids, Rev. Mod. Phys. **86**, 253 (2014).

[63] J. Heyd, G. E. Scuseria, and M. Ernzerhof, Hybrid functionals based on a screened coulomb potential, J. Chem. Phys. **118**, 8207 (2003).

[64] H. J. Monkhorst and J. D. Pack, Special points for brillouin-zone integrations, Phys. Rev. B **13**, 5188 (1976).

[65] W. Kohn and L. J. Sham, Self-consistent equations including exchange and correlation effects, Phys. Rev. **140**, A1133 (1965).

[66] Y. Wei, X. Li, J. Yang, C. Liu, J. Zhao, Y. Liu, and S. Dong, Interaction between hydrogen and gallium vacancies in β-Ga_2O_3, Sci. Rep. **8**, 10142 (2018).

[67] M. Ferrero, M. Rérat, R. Orlando, and R. Dovesi, The calculation of static polarizabilities of 1–3d periodic compounds. the implementation in the CRYSTAL code, J. Comput. Chem. **29**, 1450 (2008).

[68] M. Ferrero, M. Rérat, R. Orlando, R. Dovesi, and I. J. Bush, Coupled perturbed Kohn–Sham calculation of static polarizabilities of periodic compounds, J. Phys.: Conf. Ser. **117**, 012016 (2008).

[69] V. Lacivita, M. Ferrero, R. Orlando, and R. Dovesi, Calculation of the dielectric constant ε and first nonlinear susceptibility $\chi^{(2)}$ of crystalline potassium dihydrogen phosphate by the coupled perturbed hartree–fock and coupled perturbed kohn–sham schemes as implemented in the crystal code, J. Chem. Phys. **131**, 204509 (2009).

[70] J. P. Perdew, K. Burke, and M. Ernzerhof, Generalized gradient approximation made simple, Phys. Rev. Lett. **77**, 3865 (1996).

[71] Z. Hao and T. Liu, Formation and transport of polarons in β-Ga_2O_3: an *Ab Initio* study, J. Phys. Chem. C **129**, 8464 (2025).

[72] E. Korhonen, F. Tuomisto, D. Gogova, G. Wagner, M. Baldini, Z. Galazka, R. Schewski, and M. Albrecht, Electrical compensation by Ga vacancies in Ga_2O_3 thin films, Appl. Phys. Lett. **106**, 242103 (2015).

[73] S. K. Swain, M. H. Weber, J. Jesenovec, M. Saleh, K. G. Lynn, and J. S. McCloy, Compensation of shallow donors by gallium vacancies in monoclinic β-Ga_2O_3, Phys. Rev. Appl. **15**, 054010 (2021).

[74] A. Karjalainen, I. Makkonen, J. Etula, K. Goto, H. Murakami, Y. Kumagai, and F. Tuomisto, Split Ga vacancies in n-type and semi-insulating β-Ga_2O_3 single crystals, Appl. Phys. Lett. **118**, 072104 (2021).

[75] D. Carrasco, E. Nieto-Piñero, M. Alonso-Orts, R. Serna, J. M. San Juan, M. L. Nó, J. Jesenovec, J. S. McCloy, E. Nogales, and B. Méndez, Temperature-dependent anisotropic refractive index in β-Ga_2O_3: Application in interferometric thermometers, Nanomaterials **13**, 1126 (2023).

[76] C. Sturm, J. Furthmüller, F. Bechstedt, R. Schmidt-Grund, and M. Grundmann, Dielectric tensor of monoclinic Ga_2O_3 single crystals in the spectral range 0.5–8.5 eV, APL Materials **3**, 106106 (2015).

[77] T. Onuma, K. A. Tanaka, K. Sasaki, S. Saito, T. Masui, T. Yamaguchi, T. Honda, A. Kuramata, and M. Higashiwaki, Electroreflectance study on optical anisotropy in β-Ga_2O_3, Appl. Phys. Lett. **115**, 231102 (2019).

[78] J. Cooke, M. Lou, M. A. Scarpulla, and B. Sensale-Rodriguez, Polarized photoluminescence from sn, fe, and unintentionally doped β-Ga_2O_3, J. Vac. Sci. Technol. A **42**, 022801 (2024).

[79] R. C. Hilborn, Einstein coefficients, cross sections, f values, dipole moments, and all that, Am. J. Phys. **50**, 982 (1982).

[80] H. Haug and A.-P. Jauho, *Quantum Kinetics in Transport and Optics of Semiconductors*, 2nd ed., Springer Series in Solid-State Sciences, Vol. 123 (Springer, 2008).

[81] K. Seeger, *Semiconductor Physics: An Introduction*, 8th ed., Advanced Texts in Physics (Springer-Verlag Berlin Heidelberg, 2002).

[82] G. Rey, C. Spindler, F. Babbe, W. Rachad, S. Siebentritt, M. Nuys, R. Carius, S. Li, and C. Platzer-Björkman, Absorption coefficient of a semiconductor thin film from photoluminescence, Phys. Rev. Appl. **9**, 064008 (2018).

[83] W. van Roosbroeck and W. Shockley, Photon-radiative recombination of electrons and holes in germanium, Phys. Rev. **94**, 1558 (1954).

[84] P. Würfel, The chemical potential of radiation, J. Phys. C: Solid State Phys. **15**, 3967 (1982).

Supplementary Files

This is a list of supplementary files associated with this preprint. Click to download.

- SpinGaOsup.pdf